

# Three-dimensional flat bands and possible interlayer triplet pairing superconductivity in the alternating twisted NbSe<sub>2</sub> moiré bulk

Shuang Liu,<sup>1,2</sup> Peng Chen,<sup>2,3,4</sup> and Shihao Zhang<sup>1,\*</sup>

<sup>1</sup>*School of Physics and Electronics, Hunan University, Changsha 410082, China*

<sup>2</sup>*Department of Physics, Guangdong Technion - Israel Institute of Technology,  
241 Daxue Road, Shantou, Guangdong 515063, China*

<sup>3</sup>*Department of Physics, Technion – Israel Institute of Technology, 32000 Haifa, Israel*

<sup>4</sup>*Guangdong Provincial Key Laboratory of Materials and Technologies for Energy Conversion,  
Guangdong Technion – Israel Institute of Technology, Guangdong 515063, China*

Moiré superlattices hosting flat bands and correlated states have emerged as a focal topic in condensed matter research. Through first-principles calculations, we investigate three-dimensional flat bands in alternating twisted NbSe<sub>2</sub> moiré bulk structures. These structures exhibit enhanced interlayer interactions compared to twisted bilayer configurations. Our results demonstrate that moiré bulks undergo spontaneous large-scale structural relaxation, resulting in the formation of remarkably flat energy bands at twist angles  $\leq 7.31^\circ$ . The  $k_z$ -dependent dispersion of flat bands across different moiré bulks reveals their intrinsic three-dimensional character. The presence of out-of-plane mirror symmetry in these moiré bulk structures suggests possible interlayer triplet superconducting pairing mechanisms that differ from those in twisted bilayer systems. Our work paves the way for exploring potential three-dimensional flat bands in other moiré bulk systems.

## INTRODUCTION

Superconductivity in electronic systems with interacting electrons is a long-standing and captivating issue in condensed matter physics. Recent breakthroughs in twisted bilayer graphene (TBG) have underscored the critical role of engineered electronic band structures, particularly flat bands near the Fermi level, in facilitating unconventional superconductivity and correlated insulating states[1–3]. This has propelled the field of twistronics, in which controlled rotational misalignment in van der Waals (vdW) structures creates moiré patterns that dramatically modify electronic structure into flat bands. Within these systems featuring flat bands, the electron-electron Coulomb interaction prevails over the kinetic energy[2–7], and thus provide a fertile platform for studying the interplay and competition of superconductivity and correlation[8–37].

In the twistronics, transition metal dichalcogenide (TMD) family has garnered significant attention[38–56]. Notably, there has been considerable interest in the three-dimensional spiral structure of TMD, involving screw dislocations, which has been successfully grown through chemical vapor deposition (CVD) experiments[57–60]. Theoretical investigations have unveiled the presence of three-dimensional (3D) flat bands in the graphite moiré bulk[61], which show the possible novel states in other 3D moiré structures.

Within the TMD family, NbSe<sub>2</sub> exhibits superconducting and charge density waves in few layers and bulk. The critical temperature of the superconducting rises with an increase in the number of layers[62], suggesting that twisted NbSe<sub>2</sub> bulk may possess a higher critical temperature compared to twisted few layers. The varying numbers of layers and twist angles in twisted NbSe<sub>2</sub> lead

to a diverse structural transition, influencing interlayer coupling and electronic characteristics. Those highlight twisted NbSe<sub>2</sub> bulk as a promising candidate for investigating 3D flat band structures and superconductivity.

In this work, using first-principles methods, we systematically studied the evolution of atom displacements, band structures and bandwidths in twisted angel ranging from  $13.17^\circ$  to  $4.41^\circ$ . The moiré bulk experiences spontaneous large-scale structural relaxation and exhibits extremely flat energy bands when twisted angle is not larger than  $7.31^\circ$ . Furthermore, the flat bands in various moiré structures exhibit a dependence on the  $k_z$  direction, indicate of three-dimensional flat bands in the alternating twisted NbSe<sub>2</sub> moiré bulk. Especially, the bandwidth at  $6.00^\circ$  is narrower than that of the  $1.05^\circ$  TBG. Moreover, the out-of-plane mirror symmetry in the moiré bulk results in a distinct interlayer triplet pairing for superconductivity, distinguishing it from the twisted NbSe<sub>2</sub> bilayer system.

## CALCULATIONS METHODS

The structure optimizations of twisted NbSe<sub>2</sub> bulk were performed using the OpenMX with the Perdew–Burke–Ernzerhof (PBE) exchange–correlation function. We used the norm-conserving pseudopotentials and pseudo-atomic orbitals Se7.0-s3p2d2 and Nb7.0-s3p2d2[63, 64]. During the structure relaxation calculations, a k-points grid of  $1 \times 1 \times 2$  is adopted. The force criterion is set to  $10^{-3}$  Hartree/Bohr. DFT-D3 method was employed to take into account vdW interactions during the structure optimizations[65].

The band structures of various twist angles were calculated by real-space electronic structure method imple-

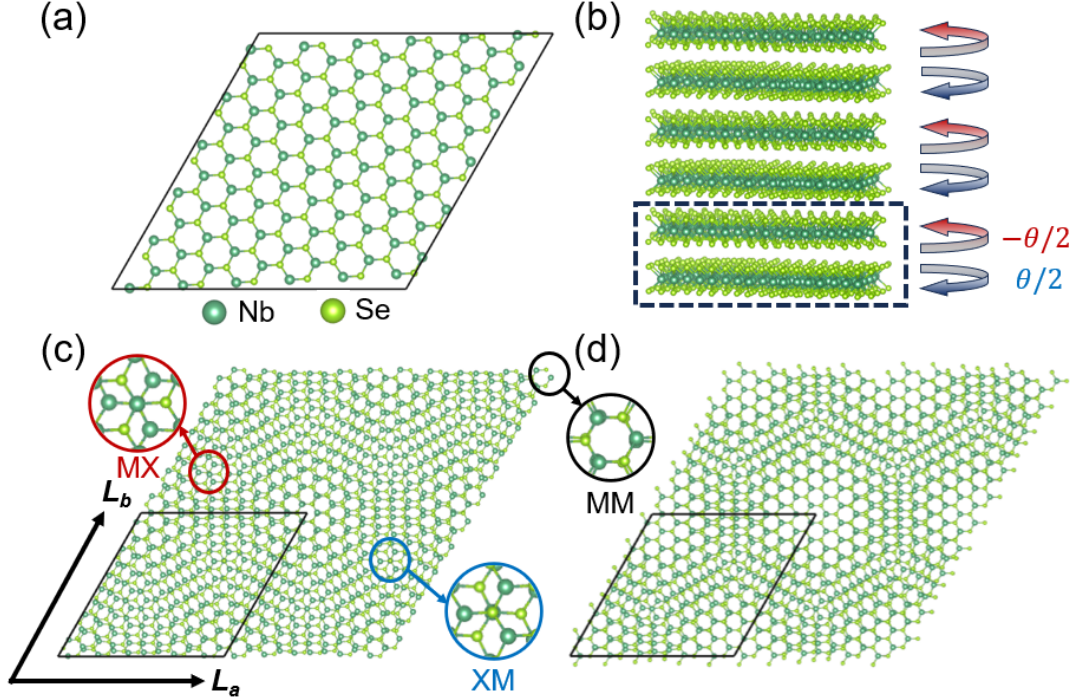


FIG. 1. (a) The top view of monolayer NbSe<sub>2</sub>. (b) The side view of alternating twisted NbSe<sub>2</sub> moiré bulk. The unit cell of moiré bulk is remarked by black dashed lines. (c) The unrelaxed structure of alternating 6.01°-twisted NbSe<sub>2</sub> moiré bulk. (d) The relaxed structure of alternating 6.01°-twisted NbSe<sub>2</sub> moiré bulk. Compared to unrelaxed structure, obvious expansion of MM region exists in the relaxed structure.

mented in the RESCU package[66]. In the self-consistent calculations, a k-points grid of  $2 \times 2 \times 4$  is adopted for twist angles ranging from 13.17° to 6.01° and  $1 \times 1 \times 4$  is adopted for 5.09° and 4.41°-twisted structures. The self-consistent procedure in the RESCU finish when the charge variation per valence electron is less than  $10^{-6}$  e. The reliability of RESCU is verified by comparing with VASP [67–70] results within the bulk and large-angle twisted NbSe<sub>2</sub> as shown in Fig. S1.

## RESULTS AND DISCUSSIONS

### Twisted bulk structures

The crystal structure of NbSe<sub>2</sub> monolayer is illustrated in Fig.1 (a), with each layer lacking inversion symmetry. In this study, we consider the moiré bulk consistent of alternating twisted NbSe<sub>2</sub> bulk as depicted in Fig.1(b). In all calculations, the out-of-plane lattice parameter is fixed to relaxed parameter of aligned bilayer 13.4Å. In these moiré bulks, only  $C_{3z}$  rotational symmetry and  $M_z$  mirror symmetry are preserved, while inversion symmetry and  $M_y$  mirror symmetry are both broken.

The lattice vectors of moiré unit cells can be described with a pair of integers  $(m, n)$ [71, 72]. One of the moiré lattice vectors can be obtained by  $L_a = ml_a + nl_b$ , where

$l_a$  and  $l_b$  are the lattice vectors corresponding to constituent monolayers. The commensurate twisted angle  $\theta$  is related to  $(m, n)$ ,

$$\cos \theta = \frac{1}{2} \frac{m^2 + n^2 + 4mn}{m^2 + n^2 + mn}. \quad (1)$$

The other moiré lattice vector  $L_b$  is obtained by rotating  $L_a$  by 60°. In our cases, we considered the twisted angle  $\theta$  within the range of 4.41° to 13.17°. The relationship between twisted angle, number of atoms and integers  $(m, n)$  in the moiré unit cell are listed in the Table.I. Fig. 1 (c) shows the unrelaxed 6.01°-twisted moiré pattern of NbSe<sub>2</sub> bulk from top view. There are three high-symmetry positions within the moiré unitcell, including MM, MX and XM staking patterns. The center of MM region is located at the original point, and the center of MX and

TABLE I. The relation between twisted angle, atoms  $N_{atoms}$  and integers  $(m, n)$  in moiré unit cell.

n	m	angle	$N_{atoms}$
2	3	13.17°	114
3	4	9.43°	222
4	5	7.34°	366
5	6	6.01°	546
6	7	5.09°	762
7	8	4.41°	1014

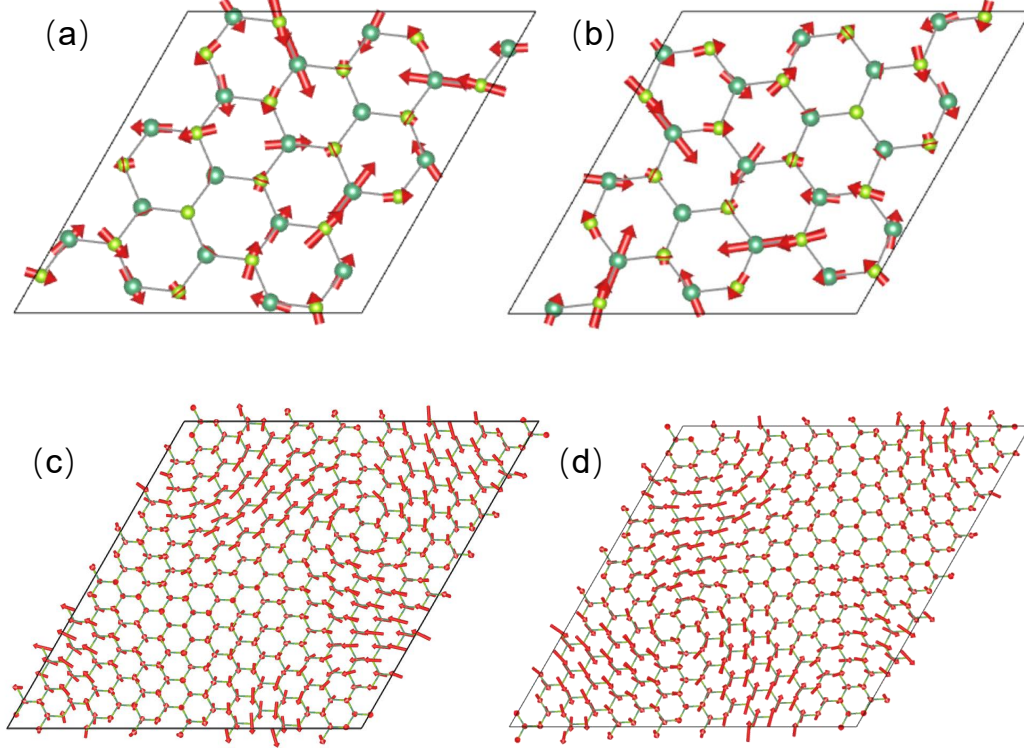


FIG. 2. The atomic displacements in the top layer (a) and bottom layer (b) in the unitcell of alternating  $13.17^\circ$ -twisted  $\text{NbSe}_2$  moiré bulk are shown, the length of red vectors on each atom refers to atomic displacement amplitude with scaling factor of 25. Here atomic displacements in the top layer (c) and bottom layer (d) in the unitcell of alternating  $4.41^\circ$ -twisted  $\text{NbSe}_2$  moiré bulk are also present with scaling factor of 3. One can see Fig. S2 for more clear displacement distributions.

XM region is  $(L_a + L_b)/3$  and  $2(L_a + L_b)/3$ , respectively. Our relaxed structure is present in the Fig. 1(d), and we can note that MM region becomes remarkably expanded compared to unrelaxed cases, while MX and XM regions reduce to domain walls in the relaxed structure.

In the relaxed structure, the atomic displacement of  $\theta=13.17^\circ$  and  $\theta=4.41^\circ$  are shown in Fig. 2. In the large-angle ( $\theta=13.17^\circ$ ) twisted structure, only a few atoms experience remarkable displacements. In the top layer, clockwise displacements occur around the MX position. In the bottom layer, anti-clockwise displacements occur around the XM site. However, in the small-angle twisted structure with  $\theta=4.41^\circ$ , distinctive vortex-like patterns of atomic displacements emerge, predominantly concentrated around the MM site, leading to the formation of a larger MM region within the moiré structure. Each layer experiences interlayer interactions from both adjacent layers, which collectively suppress significant out-of-plane corrugation in the moiré bulk structure. The results of atomic displacement are consistent with Ref [73], and reveal that remarkable vortex-like spontaneous displacement in the moiré bulk structure.

### Electronic properties

To study the three-dimensional electronic structure of twisted  $\text{NbSe}_2$  bulk, we calculated the band structures on different  $k_x - k_y$  planes across the Brillouin zone ( $k_z = 0, \pi/3, \pi/2$ ). As shown in Fig. 3, the energy bands near Fermi level are all  $k_z$ -dependent in the alternating twisted  $\text{NbSe}_2$  moiré bulk.

In the unrelaxed structure of alternating twisted  $\text{NbSe}_2$  moiré bulk with  $\theta = 13.17^\circ, 9.43^\circ, 7.32^\circ$  and  $6.01^\circ$ , there exist hole pockets located at  $\Gamma$  point. However, in the relaxed structure, hole pockets are only maintained in the twisted  $\text{NbSe}_2$  moiré bulk with  $\theta = 13.17^\circ$  and  $9.43^\circ$  twist angles. This difference arises because energy bands become more dispersionless in the relaxed structure with smaller twist angle. Especially, large bandgaps at  $\Gamma$ -point disappear in the relaxed structure, and more electronic states occur near the Fermi level in the alternating twisted  $\text{NbSe}_2$  moiré bulk with twist angle  $\theta \leq 7.34^\circ$ . These results reveal that structural spontaneous relaxations in the alternating twisted  $\text{NbSe}_2$  moiré bulk play an important role in their electronic structures.

We note that lattice relaxation in the twisted bilayer graphene leads to gap opening at  $\pm 4$  filling and particle-hole asymmetry[74–77]. However, atomic relaxation fails



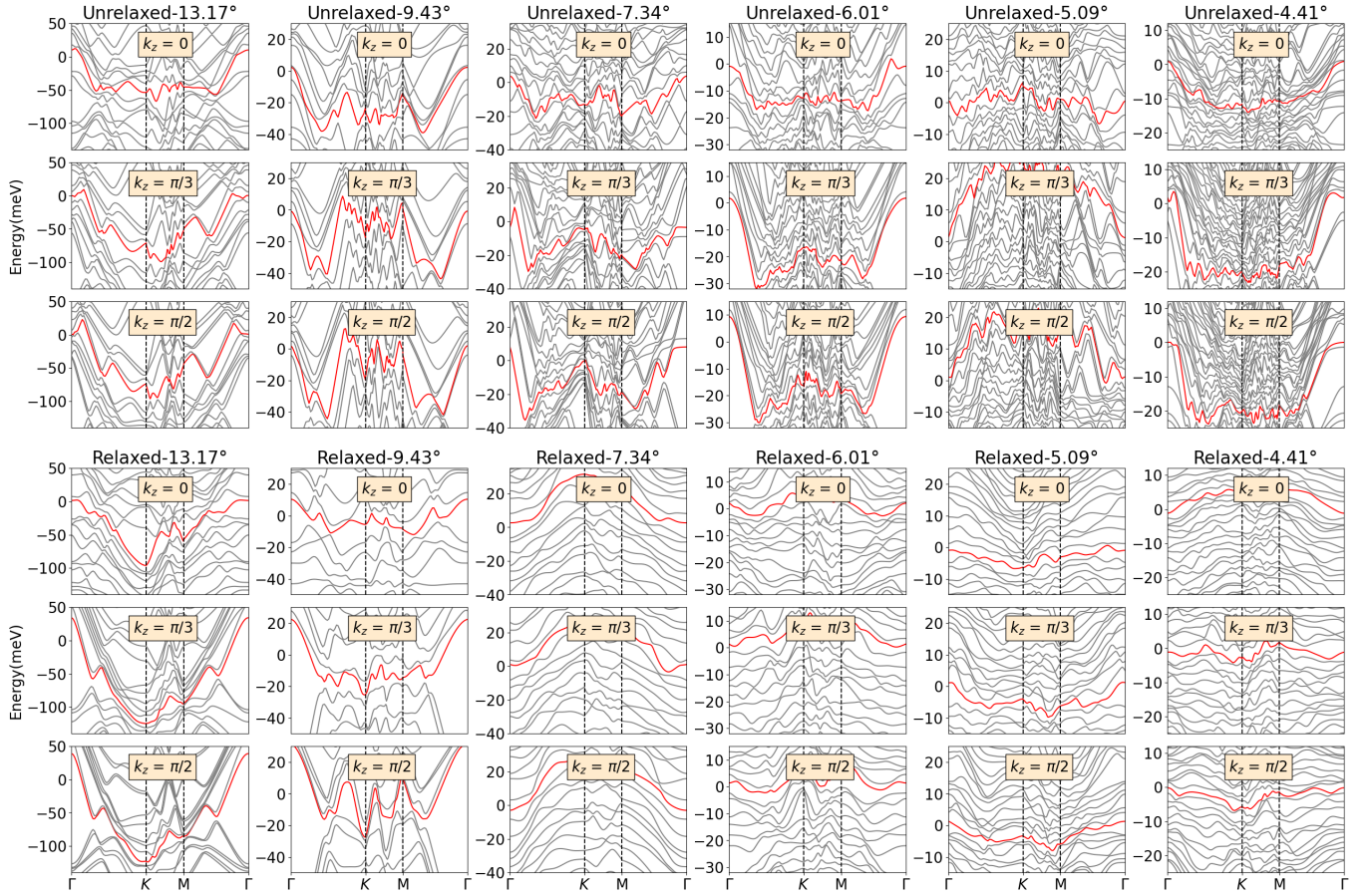


FIG. 3. The energy bands of alternating twisted NbSe<sub>2</sub> moiré bulk with unrelaxed and relaxed structures. Here we highlighted the energy bands whose energy is closest to Fermi level.

to form similarly isolated flat bands in the twisted NbSe<sub>2</sub> bulk, which may be attributed to strong intralayer hopping and large intrinsic bandwidth of NbSe<sub>2</sub> compared to interlayer interaction.

In the NbSe<sub>2</sub> monolayer, the energy bands in the  $\Gamma$  valley originate from  $d_z^2$  orbitals, but in the K valley, energy bands are mainly contributed by  $d_{xy} + d_{x^2-y^2}$  orbitals[78]. Orbital projection analysis for the 21.79° twisted bulk (Fig. S4) confirms that the flat bands proximate to the Fermi energy exhibit K-valley character, dominated by the  $d_{xy} + d_{x^2-y^2}$  orbitals.

It is noted that there are two different configurations in the twisted transition-metal dichalcogenides (TMD), which centers on the MM region and MX region[79]. In the MX-stacking twisted TMD, one layer is obtained by rotating by 180° around the hollow compared to MM-stacking twisted TMD. Previous work[79] showed that the electronic structures behave very different in these twisted structure. Thus, we also calculated the electronic structure of 13.17° and 6.01° with AP centered twisted structure as shown in Fig. 4. Although the overall band shapes differ significantly between the MX- and MM-centered twisting structures, the bandwidths of the

bands near the Fermi energy remain similar: 93.3 meV (MX) vs. 102.3 meV (MM) for 13.17°, and 12.6 meV (MX) vs. 11.1 meV (MM) for 6.01°. These results indicate that the bandwidths of the bands near the Fermi energy is mainly insensitive to the twisting center.

To trace the evolution of the bandwidth with decreasing twist angle, we focus on the bands closest to the Fermi level. The average bandwidth of these bands at different  $k_z$  is used as an indicator of the system's overall bandwidth. As shown in Fig.5, the bandwidths of alternating 7.34°-twisted NbSe<sub>2</sub> moiré bulk decrease to 30 meV. Subsequently, in the alternating 6.01°-twisted NbSe<sub>2</sub> moiré bulk, the bandwidths are further reduced to 10 meV, which are close to typical bandwidths of magic-angle twisted bilayer graphene as shown in the Fig.5. Thus, three-dimensional flat bands emerge in the alternating twisted NbSe<sub>2</sub> moiré bulk with twisted angle  $\theta \leq 6.01^\circ$ , which can experience significant electron-electron interaction. In the alternating twisted NbSe<sub>2</sub> moiré bulk, each layer possesses interlayer interaction from two neighboring layers. But in the twisted bilayer NbSe<sub>2</sub> or at the surface of moiré bulk, these interlayer interactions weaken, leading to an enhancement in the bandwidth of moiré

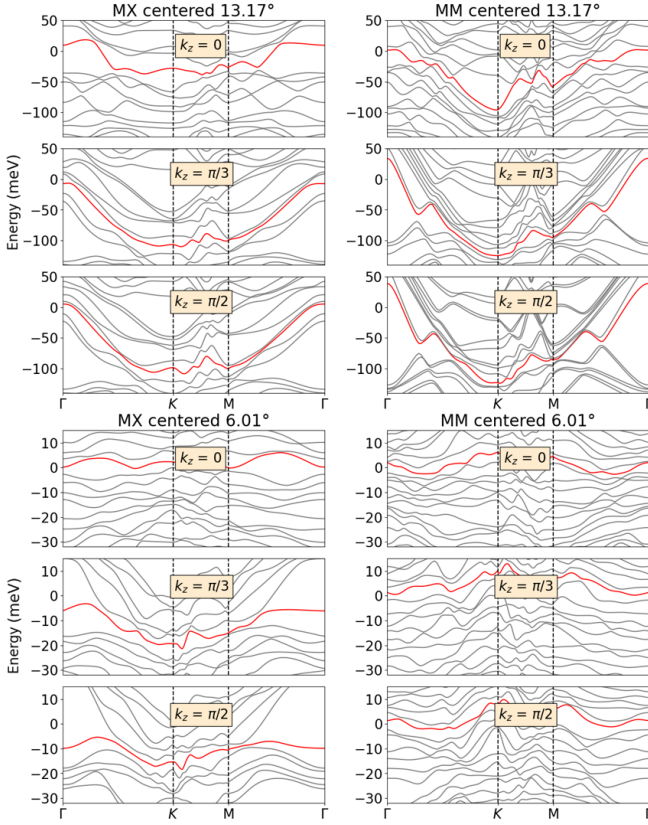


FIG. 4. Band structures in twisted 13.17° and 6.01°  $\text{NbSe}_2$  with a rotation center of MX and MM (result of main text) respectively.

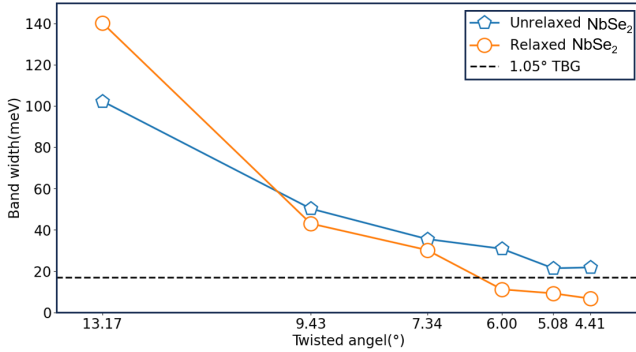


FIG. 5. The average bandwidths of energy bands highlighted in the Fig.3 in different alternating twisted  $\text{NbSe}_2$  moiré bulk.

bands. Thus, the surface state behaves different from bulk states in the alternating twisted  $\text{NbSe}_2$  moiré bulk.

### Electron Coulomb interaction

The electron Coulomb interaction can be written as  $H = V(q)c_{k+q}^\dagger c_{k'-q}^\dagger c_{k'} c_k$ , where  $k, k', q$  are wave vectors in the Brillouin zone. In the 2D cases,  $V(q) =$

$e^2/(2\Omega_M \epsilon \epsilon_0 \sqrt{q^2 + \kappa^2})$  denotes the screened Coulomb interaction, where  $\Omega_M$  is the area of moiré lattice,  $\kappa$  is the inverse screening length, and  $\epsilon$  denotes the background dielectric constant. But in the 3D cases,  $V(q) = e^2/[d\Omega_M \epsilon \epsilon_0 (q^2 + \kappa^2)]$  where  $d$  refers to out-of-plane lattice constant. In the experiments,  $\kappa = 0.002 \sim 0.02 \text{ \AA}^{-1}$ . We can note that at the small  $q$  (meets  $d\sqrt{q^2 + \kappa^2} < 2$ ), electron interaction in the 3D case is stronger than that in the 2D twisted system. In the 6.01° twisted  $\text{NbSe}_2$  moiré bulk, when  $q \sim 0.1G = 0.022 \text{ \AA}^{-1}$  ( $G$  is in-plane reciprocal lattice vector length) and  $\kappa = 0.01 \text{ \AA}^{-1}$ ,  $\frac{2}{d\sqrt{q^2 + \kappa^2}} = 6.1762$  reveals that the 3D electron Coulomb interaction is about 6 times as large as that of 2D electron interaction. Especially, 3D electron Coulomb interaction delays rapidly with  $\sim 1/q^2$  power law, and we note that  $V(q = 0.1G)/V(q = 0.316G) = 10$  indicates of short-range electron interaction. Thus, the dominant electron Coulomb interaction in the 3D moiré system originates from small- $q$  interaction term. Despite of multiband electronic structure near the Fermi level, dominant electron interaction are limited to small- $q$  scattering, whose region includes only one or two energy bands.

In the case of alternating twisted trilayer graphene, flat bands coexist with highly dispersive Dirac cones[80, 81]. These bands overlap near the Fermi level. Despite this, experiments have observed correlated states within this moiré system. Theoretical work[82] has also investigated these states, referring to them as intervalley coherent states. Therefore, the presence of correlated states in the alternating twisted trilayer graphene demonstrates that overlapping bands do not suppress the correlated state within the flat bands. Thus, multi-band scattering or excitation may not suppress the correlated states in our alternating twisted bulk.

It is noted that the supercell is enlarged with the decrease of twist angle. At the same time, the effect of band folding is evident to reduce the bandwidths. We define the characteristic energy on the moiré length as  $U_M = e^2/(4\pi\epsilon\epsilon_0 L_S)$ [23]. The comparison between characteristic interaction energy and bandwidth can give out proper scale analysis. In the magic-angle twisted bilayer graphene, the characteristic energy is about 22 meV, which is larger than the bandwidth of flat bands. As for 6.01° twisted  $\text{NbSe}_2$  moiré bulk, the reciprocal lattice length is 4 times as large as that of magic-angle twisted bilayer graphene. Thus, the characteristic energy is about 88 meV, which is much larger than the bandwidths of energy bands. These scale analysis show that 6.01 twisted  $\text{NbSe}_2$  moiré bulk resides in the strong interaction regime favorable for correlated electron physics.

## Interlayer triplet pairing superconductivity

NbSe<sub>2</sub> always exhibits superconductivity in few layers and bulk. Here we discuss the possible superconductivity in the alternating twisted NbSe<sub>2</sub> moiré bulk. In the superconducting materials, the electrodynamic characteristics are expressed by

$$\mathbf{j} = -D_s \mathbf{A}. \quad (2)$$

Here  $\mathbf{j}$  is current density,  $\mathbf{A}$  denotes vector potential and  $D_s$  refers to superfluid weight. The superfluid weight is crucial criterion of superconductivity. It can be divided into two sections: conventional contribution and geometric contribution[10]. The conventional contribution is driven from single-band model, but geometric contribution originates from multi-band framework[10]. In the flat-band system, geometric superfluid weight predominates over conventional superfluid weight. Thus, in the alternating twisted NbSe<sub>2</sub> bulk with smaller twist angles, geometric superfluid weight plays a more significant role. While the increased effective mass suggests enhanced band flatness, a key indicator for superconductivity, it is crucial to note that the geometric superfluid weight depends not only on the effective mass but also sensitively on the geometric properties of the electronic wavefunctions[83]. The influence of wavefunction geometry on superconductivity within the alternating twisted NbSe<sub>2</sub> bulk requires further dedicated investigation in future work.

Now we discuss possible superconducting pairings in the alternating twisted NbSe<sub>2</sub> bulk. The continuum Hamil-

tonian for the superconducting part can be expressed as

$$H_{sc}(\mathbf{r}) = \int d\mathbf{r} \sum_{\xi l l' s s'} \psi_{\xi l s}^\dagger(\mathbf{r}) \Delta_{ll', ss'}(\mathbf{r}) \psi_{-\xi l' s'}^\dagger(\mathbf{r}) + h.c.$$

Here  $\xi$  refers to valley index and  $l$  or  $l'$  represents the layer in the unitcell of moiré bulk. Following the previous work[84, 85], we only consider momentum-direction-independent interaction pairings in this work, for simplicity. The electronic band structure only indicates of single-particle wavefunction, so we need to determine the certain form of interaction pairing by symmetry constraint.

To begin, we analyze the possible superconducting pairings in the twisted bilayer NbSe<sub>2</sub>. In the twisted bilayer NbSe<sub>2</sub>, the system exhibits  $\mathcal{T} \times D_3$  symmetry[85]. Thus, twisted bilayer NbSe<sub>2</sub> has time-reversal symmetry  $\mathcal{T} = i s_y \mathcal{K}$ , three-fold rotational symmetry  $C_{3z} = e^{i 2\pi s_z / 3}$  and two-fold rotational symmetry  $C_{2y} = -i \tau_x s_y$ . Here  $\tau$  and  $s$  are Pauli matrices defined in layer and spin space, respectively. There are only six matrices of pairing wavefunction:  $s_y$ ,  $\tau_x s_y$ ,  $\tau_z s_y$ ,  $\tau_y$ ,  $\tau_y s_x$ ,  $\tau_y s_z$  can couple to the s-wave pairings. Among these possible pairings, only  $\{\tau_y, \tau_y s_z\}$  pairing belongs to two-dimensional irreducible representation, and other pairings belong to one-dimensional irreducible representation. The  $(\tau_0, \tau_x) s_y$ ,  $\tau_z s_y$ , and  $\tau_y s_x$  describe the singlet pairings, and  $\{\tau_y, \tau_y s_z\}$  refers to triplet pairing. However, in the alternating twisted NbSe<sub>2</sub> bulk, extra mirror symmetry  $M_z = i s_z$  rule out all pairings of one-dimensional irreducible representation. Thus, only  $\{\tau_y, \tau_y s_z\}$  pairing is possible in the alternating twisted NbSe<sub>2</sub> bulk, whose explicit pairing form is

$$\Psi_{BCS} = \{\psi_{-\xi-\mathbf{k}, l\uparrow} \psi_{\xi+\mathbf{k}, l'\uparrow} + \psi_{-\xi-\mathbf{k}, l\downarrow} \psi_{\xi+\mathbf{k}, l'\downarrow}, \psi_{-\xi-\mathbf{k}, l\uparrow} \psi_{\xi+\mathbf{k}, l'\uparrow} - \psi_{-\xi-\mathbf{k}, l\downarrow} \psi_{\xi+\mathbf{k}, l'\downarrow}\} \quad (l \neq l'). \quad (3)$$

Thus, only interlayer triplet pairing can exist in the alternating twisted NbSe<sub>2</sub> bulk, which is different from twisted bilayer system.

We note that the minimal structural platform exhibiting the crucial mirror symmetry discussed here would be the alternating twisted trilayer system. For instance, alternating twisted trilayer graphene has been proposed as a promising platform for realizing spin-triplet pairing superconductivity, largely attributed to its mirror symmetry[86]. Similarly, alternating twisted trilayer NbSe<sub>2</sub> would also possess mirror symmetry and could potentially support triplet pairing. However, a significant experimental consideration is that such trilayer systems are inherently sensitive to substrate effects, which typically break the mirror symmetry. In contrast, the bulk nature of the alternating twisted moiré system investigated in this work offers inherent protection for its bulk

states against such symmetry-breaking substrate potentials, potentially providing a more robust environment for realizing symmetry-protected phenomena.

## CONCLUSION

In summary, we studied three-dimensional flat bands in the alternating twisted NbSe<sub>2</sub> moiré bulk by first-principles calculations. Unlike the twisted bilayer system, each layer in the moiré bulk experiences stronger interlayer interactions. Our calculations reveal that the moiré bulk undergoes spontaneous large-scale structural relaxation and exhibits remarkably flat energy bands when twist angle is not larger than 7.31°. The flat bands in various moiré bulks behave  $k_z$ -dependent, indicate of three-dimensional flat bands in the alternating twisted

NbSe<sub>2</sub> moiré bulk. The out-of-plane mirror symmetry in the moiré bulk make its unique interlayer triplet pairing of superconductivity different from twisted bilayer system.

## ACKNOWLEDGMENTS

This work was supported by the National Key Research and Development Program of China (No. 2024YFA1410300), the National Natural Science Foundation of China (No. 12304217), the Natural Science Foundation of Hunan Province (No. 2025JJ60002) and the Fundamental Research Funds for the Central Universities from China (No. 531119200247). We gratefully acknowledge HZWTECH for providing computation facilities.

---

\* zhangshh@hnu.edu.cn

- [1] H. Aoki, *Journal of Superconductivity and Novel Magnetism* **33**, 2341 (2020).
- [2] Y. Cao, V. Fatemi, S. Fang, K. Watanabe, T. Taniguchi, E. Kaxiras, and P. Jarillo-Herrero, *Nature* **556**, 43 (2018).
- [3] Y. Cao, V. Fatemi, A. Demir, S. Fang, S. L. Tomarken, J. Y. Luo, J. D. Sanchez-Yamagishi, K. Watanabe, T. Taniguchi, E. Kaxiras, R. C. Ashoori, and P. Jarillo-Herrero, *Nature* **556**, 80 (2018).
- [4] Y. Tang, L. Li, T. Li, Y. Xu, S. Liu, K. Barmak, K. Watanabe, T. Taniguchi, A. H. MacDonald, J. Shan, and K. F. Mak, *Nature* **579**, 353 (2020).
- [5] E. C. Regan, D. Wang, C. Jin, M. I. Bakti Utama, B. Gao, X. Wei, S. Zhao, W. Zhao, Z. Zhang, K. Yumigeta, M. Blei, J. D. Carlström, K. Watanabe, T. Taniguchi, S. Tongay, M. Crommie, A. Zettl, and F. Wang, *Nature* **579**, 359 (2020).
- [6] L. Wang, E.-M. Shih, A. Ghiotto, L. Xian, D. A. Rhodes, C. Tan, M. Claassen, D. M. Kennes, Y. Bai, B. Kim, K. Watanabe, T. Taniguchi, X. Zhu, J. Hone, A. Rubio, A. N. Pasupathy, and C. R. Dean, *Nature Materials* **19**, 861 (2020).
- [7] G. Pasquale, Z. Sun, K. Čerņevičs, R. Perea-Causin, F. Tagarelli, K. Watanabe, T. Taniguchi, E. Malic, O. V. Yazyev, and A. Kis, *Nano Letters* **22**, 8883 (2022).
- [8] P. Wilhelm, T. C. Lang, and A. M. Läuchli, *Physical review. B/Physical review. B* **103**, 10.1103/physrevb.103.125406 (2021).
- [9] Y. Zhang, Y.-W. Tan, H. L. Stormer, and P. Kim, *Nature* **438**, 201–204 (2005).
- [10] P. Törmä, S. Peotta, and B. A. Bernevig, *Nature Reviews Physics* **4**, 528 (2022).
- [11] J. Y. Lee, E. Khalaf, S. Liu, X. Liu, Z. Hao, P. Kim, and A. Vishwanath, *Nature communications* **10**, 5333 (2019).
- [12] F. Wu, A. H. MacDonald, and I. Martin, *Physical review letters* **121**, 257001 (2018).
- [13] E. Codecido, Q. Wang, R. Koester, S. Che, H. Tian, R. Lv, S. Tran, K. Watanabe, T. Taniguchi, F. Zhang, M. Bockrath, and C. N. Lau, *Science Advances* **5**, 10.1126/sciadv.aaw9770 (2019).
- [14] X. Lu, P. Stepanov, W. Yang, M. Xie, M. A. Aamir, I. Das, C. Urgell, K. Watanabe, T. Taniguchi, G. Zhang, A. Bachtold, A. H. MacDonald, and D. K. Efetov, *Nature* **574**, 653 (2019).
- [15] P. Stepanov, I. Das, X. Lu, A. Fahimniya, K. Watanabe, T. Taniguchi, F. H. L. Koppens, J. Lischner, L. Levitov, and D. K. Efetov, *Nature* **583**, 375 (2020).
- [16] Y. Saito, J. Ge, K. Watanabe, T. Taniguchi, and A. F. Young, *Nature Physics* **16**, 926 (2020).
- [17] X. Liu, Z. Wang, K. Watanabe, T. Taniguchi, O. Vafek, and J. Li, *Science* **371**, 1261 (2021).
- [18] Y. Cao, D. Rodan-Legrain, J. M. Park, N. F. Yuan, K. Watanabe, T. Taniguchi, R. M. Fernandes, L. Fu, and P. Jarillo-Herrero, *science* **372**, 264 (2021).
- [19] J. Kang and O. Vafek, *Phys. Rev. Lett.* **122**, 246401 (2019).
- [20] K. Seo, V. N. Kotov, and B. Uchoa, *Phys. Rev. Lett.* **122**, 246402 (2019).
- [21] M. Xie and A. H. MacDonald, *Phys. Rev. Lett.* **124**, 097601 (2020).
- [22] N. Bultinck, S. Chatterjee, and M. P. Zaletel, *Phys. Rev. Lett.* **124**, 166601 (2020).
- [23] S. Zhang, X. Dai, and J. Liu, *Phys. Rev. Lett.* **128**, 026403 (2022).
- [24] S. Zhang, X. Lu, and J. Liu, *Phys. Rev. Lett.* **128**, 247402 (2022).
- [25] N. Bultinck, E. Khalaf, S. Liu, S. Chatterjee, A. Vishwanath, and M. P. Zaletel, *Phys. Rev. X* **10**, 031034 (2020).
- [26] J. Liu and X. Dai, *Phys. Rev. B* **103**, 035427 (2021).
- [27] Y. Zhang, K. Jiang, Z. Wang, and F. Zhang, *Phys. Rev. B* **102**, 035136 (2020).
- [28] K. Hejazi, X. Chen, and L. Balents, *Phys. Rev. Research* **3**, 013242 (2021).
- [29] J. Kang and O. Vafek, *Phys. Rev. B* **102**, 035161 (2020).
- [30] B.-B. Chen, Y. D. Liao, Z. Chen, O. Vafek, J. Kang, W. Li, and Z. Y. Meng, *Nature Communications* **12**, 5480 (2021).
- [31] Y. Da Liao, J. Kang, C. N. Breiør, X. Y. Xu, H.-Q. Wu, B. M. Andersen, R. M. Fernandes, and Z. Y. Meng, *Phys. Rev. X* **11**, 011014 (2021).
- [32] B. A. Bernevig, Z.-D. Song, N. Regnault, and B. Lian, *Phys. Rev. B* **103**, 205413 (2021).
- [33] B. Lian, Z.-D. Song, N. Regnault, D. K. Efetov, A. Yazdani, and B. A. Bernevig, *Phys. Rev. B* **103**, 205414 (2021).
- [34] F. Xie, A. Cowsik, Z.-D. Song, B. Lian, B. A. Bernevig, and N. Regnault, *Phys. Rev. B* **103**, 205416 (2021).
- [35] T. Soejima, D. E. Parker, N. Bultinck, J. Hauschild, and M. P. Zaletel, *Phys. Rev. B* **102**, 205111 (2020).
- [36] X. Zhang, G. Pan, Y. Zhang, J. Kang, and Z. Y. Meng, *Chinese Physics Letters* **38**, 077305 (2021).
- [37] D. E. Parker, T. Soejima, J. Hauschild, M. P. Zaletel, and N. Bultinck, *Phys. Rev. Lett.* **127**, 027601 (2021).
- [38] C. Xu, J. Li, Y. Xu, Z. Bi, and Y. Zhang, *Proceedings of the National Academy of Sciences* **121**, e2316749121 (2024).
- [39] N. Mao, C. Xu, J. Li, T. Bao, P. Liu, Y. Xu, C. Felser, L. Fu, and Y. Zhang, *Communications Physics* **7**, 262 (2024).
- [40] Y. Zhang, T. Liu, and L. Fu, *Physical Review B* **103**, 155142 (2021).

- [41] C. Xu, N. Mao, T. Zeng, and Y. Zhang, *Phys. Rev. Lett.* **134**, 066601 (2025).
- [42] F. Xu, Z. Sun, T. Jia, C. Liu, C. Xu, C. Li, Y. Gu, K. Watanabe, T. Taniguchi, B. Tong, J. Jia, Z. Shi, S. Jiang, Y. Zhang, X. Liu, and T. Li, *Phys. Rev. X* **13**, 031037 (2023).
- [43] F.-R. Fan, C. Xiao, and W. Yao, *Physical Review B* **109**, L041403 (2024).
- [44] Q. Tong, H. Yu, Q. Zhu, Y. Wang, X. Xu, and W. Yao, *Nature Physics* **13**, 356 (2017).
- [45] A. P. Reddy, T. Devakul, and L. Fu, *Phys. Rev. Lett.* **131**, 246501 (2023).
- [46] D. N. Sheng, A. P. Reddy, A. Abouelkomsan, E. J. Bergholtz, and L. Fu, *Phys. Rev. Lett.* **133**, 066601 (2024).
- [47] F. Xu, X. Chang, J. Xiao, Y. Zhang, F. Liu, Z. Sun, N. Mao, N. Peshcherenko, J. Li, K. Watanabe, *et al.*, *Nature Physics*, 1 (2025).
- [48] X.-W. Zhang, C. Wang, X. Liu, Y. Fan, T. Cao, and D. Xiao, *Nature Communications* **15**, 4223 (2024).
- [49] A. P. Reddy, F. Alsallom, Y. Zhang, T. Devakul, and L. Fu, *Phys. Rev. B* **108**, 085117 (2023).
- [50] Y.-M. Xie, C.-P. Zhang, J.-X. Hu, K. F. Mak, and K. T. Law, *Phys. Rev. Lett.* **128**, 026402 (2022).
- [51] H. Pan, M. Xie, F. Wu, and S. Das Sarma, *Phys. Rev. Lett.* **129**, 056804 (2022).
- [52] B. Li and F. Wu, *Phys. Rev. B* **111**, 125122 (2025).
- [53] W.-X. Qiu, B. Li, X.-J. Luo, and F. Wu, *Phys. Rev. X* **13**, 041026 (2023).
- [54] F. Wu, T. Lovorn, E. Tutuc, I. Martin, and A. H. MacDonald, *Phys. Rev. Lett.* **122**, 086402 (2019).
- [55] B. Li, W.-X. Qiu, and F. Wu, *Phys. Rev. B* **109**, L041106 (2024).
- [56] J. Cai, E. Anderson, C. Wang, X. Zhang, X. Liu, W. Holtzmann, Y. Zhang, F. Fan, T. Taniguchi, K. Watanabe, *et al.*, *Nature* **622**, 63 (2023).
- [57] L. Zhang, K. Liu, A. B. Wong, J. Kim, X. Hong, C. Liu, T. Cao, S. G. Louie, F. Wang, and P. Yang, *Nano letters* **14**, 6418 (2014).
- [58] P. Ci, Y. Zhao, M. Sun, Y. Rho, Y. Chen, C. P. Grigoriopoulos, S. Jin, X. Li, and J. Wu, *Nano letters* **22**, 9027 (2022).
- [59] X. Fan, Y. Jiang, X. Zhuang, H. Liu, T. Xu, W. Zheng, P. Fan, H. Li, X. Wu, X. Zhu, *et al.*, *ACS nano* **11**, 4892 (2017).
- [60] J. Chen, Y. Bai, M. Qi, W. Zhang, C. Qin, X. Fan, and L. Xiao, *Advanced Materials* **37**, 2415214 (2025).
- [61] X. Lu, B. Xie, Y. Yang, Y. Zhang, X. Kong, J. Li, F. Ding, Z.-J. Wang, and J. Liu, *Physical Review Letters* **132**, 056601 (2024).
- [62] N. E. Staley, J. Wu, P. Eklund, Y. Liu, L. Li, and Z. Xu, *Phys. Rev. B* **80**, 184505 (2009).
- [63] T. Ozaki, *Phys. Rev. B* **67**, 155108 (2003).
- [64] T. Ozaki and H. Kino, *Phys. Rev. B* **69**, 195113 (2004).
- [65] S. Grimme, J. Antony, S. Ehrlich, and H. Krieg, *The Journal of Chemical Physics* **132**, 154104 (2010).
- [66] V. Michaud-Rioux, L. Zhang, and H. Guo, *Journal of Computational Physics* **307**, 593 (2016).
- [67] G. Kresse and J. Hafner, *Physical Review B* **47**, 558–561 (1993).
- [68] G. Kresse and J. Hafner, *Physical Review B* **49**, 14251–14269 (1994).
- [69] G. Kresse and J. Furthmüller, *Physical Review B* **54**, 11169–11186 (1996).
- [70] G. Kresse and D. Joubert, *Physical Review B* **59**, 1758–1775 (1999).
- [71] P. Moon and M. Koshino, *Phys. Rev. B* **85**, 195458 (2012).
- [72] E. J. Mele, *Phys. Rev. B* **81**, 161405 (2010).
- [73] C. T. S. Cheung, Z. A. H. Goodwin, Y. Han, J. Lu, A. A. Mostofi, and J. Lischner, *Nano Letters* **24**, 12088 (2024), pMID: 39297477.
- [74] F. Guinea and N. R. Walet, *Physical Review B* **99**, 10.1103/physrevb.99.205134 (2019).
- [75] W. Miao, C. Li, X. Han, D. Pan, and X. Dai, *Physical Review B* **107**, 10.1103/physrevb.107.125112 (2023).
- [76] K. Uchida, S. Furuya, J.-I. Iwata, and A. Oshiyama, *Physical Review B* **90**, 10.1103/physrevb.90.155451 (2014).
- [77] B. Xie and J. Liu, *Physical Review B* **108**, 10.1103/physrevb.108.094115 (2023).
- [78] D. Wickramaratne, S. Khmelevskiy, D. F. Agterberg, and I. Mazin, *Physical Review X* **10**, 10.1103/physrevx.10.041003 (2020).
- [79] V. Enaldiev, V. Zólyomi, C. Yelgel, S. Magorrian, and V. Fal’ko, *Physical Review Letters* **124**, 10.1103/physrevlett.124.206101 (2020).
- [80] H. Kim, Y. Choi, É. Lantagne-Hurtubise, C. Lewandowski, A. Thomson, L. Kong, H. Zhou, E. Baum, Y. Zhang, L. Holleis, K. Watanabe, T. Taniguchi, A. F. Young, J. Alicea, and S. Nadj-Perge, *Nature* **623**, 942 (2023).
- [81] C. Shen, P. J. Ledwith, K. Watanabe, T. Taniguchi, E. Khalaf, A. Vishwanath, and D. K. Efetov, *Nature Materials* **22**, 316 (2023).
- [82] M. Christos, S. Sachdev, and M. S. Scheurer, *Phys. Rev. X* **12**, 021018 (2022).
- [83] Z. Han, J. Herzog-Arbeitman, B. A. Bernevig, and S. A. Kivelson, *Physical Review X* **14**, 10.1103/physrevx.14.041004 (2024).
- [84] Y. S. Gani, H. Steinberg, and E. Rossi, *Physical Review B* **99**, 10.1103/physrevb.99.235404 (2019).
- [85] Y.-M. Xie and K. T. Law, *Phys. Rev. Lett.* **131**, 016001 (2023).
- [86] W. Qin and A. H. MacDonald, *Phys. Rev. Lett.* **127**, 097001 (2021).